

Recurrent Variational Approach to the Two-Leg Hubbard Ladder

Eugene H. Kim

Department of Physics, University of California, Santa Barbara, California 93106-9530

Germán Sierra

Instituto de Matemáticas y Física Fundamental, C.S.I.C., 28006 Madrid, Spain

Daniel Duffy

Department of Physics, University of California, Santa Barbara, California 93106-9530

We applied the Recurrent Variational Approach to the two-leg Hubbard ladder. At half-filling, our variational Ansatz was a generalization of the resonating valence bond state. At finite doping, hole pairs were allowed to move in the resonating valence bond background. The results obtained by the Recurrent Variational Approach were compared with results from Density Matrix Renormalization Group.

I. INTRODUCTION

In the hope to get a better understanding of strongly interacting systems, there has been considerable interest in ladder systems.¹ These ladder systems have proven to be a theoretical wonderland, both analytically² and numerically.³ However, much of the analytic work done on ladders has been in weak coupling (or perturbatively in some parameter), namely because there are very few analytic methods at strong coupling. Exact diagonalization, Monte Carlo, and Density Matrix Renormalization Group methods have been the primary tools for studying these systems at strong coupling. Each of these methods has both strengths and weaknesses when considering the lattice sizes, temperatures, and couplings one can consider.

With the ability to fabricate these materials,⁴ ladders are not just a theoretical playground. For example, in $(VO)_2P_2O_7$, there are well separated two-leg ladders composed of VO_4 .⁵ Also the cuprate-like material $SrCu_2O_3$ consists of weakly coupled CuO_2 two-leg ladders,⁶ and the material $Sr_2Cu_3O_5$ consists of weakly coupled CuO_2 three-leg ladders.⁷

Recently, a powerful analytic method was developed to deal with strongly coupled quasi-one dimensional systems — the Recurrent Variational Approach (RVA).^{8,9} This method is similar in spirit to Wilson's Numerical Renormalization Group¹⁰ and White's Density Matrix Renormalization Group (DMRG).¹¹ The key idea in all of these methods is to build up the system by adding on sites at the boundary. However, the real power of the RVA is that, though analytic, the physics of the problem is taken into account in an unbiased way and elucidated quite clearly. For example, the importance of different configurations in the ground state wave function is determined without any outside assumptions, and the physics of these configurations is made clear.

In this work, we apply the RVA to the two-leg Hubbard ladder at strong coupling and small dopings. Though a considerable amount of work has been done on the Hubbard ladder and many of its properties are known, we are unaware of any work which has put this information

together and constructed a ground state wave function. Our goal in this work is to provide a simple physical picture of what the ground state might look like and to go ahead and construct a ground state wave function.

The Hamiltonian of the two-leg Hubbard ladder is given by

$$H = -t \sum_{\mathbf{i},s} (c_{\mathbf{i},s}^\dagger c_{\mathbf{i}+\hat{\mathbf{x}},s} + h.c.) - t_\perp \sum_{\mathbf{i},s} (c_{\mathbf{i},s}^\dagger c_{\mathbf{i}+\hat{\mathbf{y}},s} + h.c.) + U \sum_{\mathbf{i}} n_{\mathbf{i},\uparrow} n_{\mathbf{i},\downarrow}, \quad (1)$$

where $c_{\mathbf{i},s}^\dagger$ creates a fermion at site \mathbf{i} with spin s , $n_{\mathbf{i},s} = c_{\mathbf{i},s}^\dagger c_{\mathbf{i},s}$, t is the hopping matrix element along the chain, t_\perp is the hopping matrix element perpendicular to the chain (i.e., along the rung), and U is the on-site Coulomb repulsion. Site \mathbf{i} has coordinates (x, y) with $1 \leq x \leq N$ and $y = 1, 2$. It will also be convenient to introduce the following two operators:

$$\Delta_{\mathbf{i},\mathbf{j}}^\dagger = c_{\mathbf{i},\uparrow}^\dagger c_{\mathbf{j},\downarrow}^\dagger + c_{\mathbf{j},\uparrow}^\dagger c_{\mathbf{i},\downarrow}^\dagger, \quad (2)$$

which creates a singlet across sites \mathbf{i} and \mathbf{j} , and

$$D_{\mathbf{i}} = c_{\mathbf{i},\uparrow}^\dagger c_{\mathbf{i},\downarrow}^\dagger, \quad (3)$$

which creates a doubly occupied site.

The rest of the paper is organized as follows. In Sec. II we consider the half-filled case. In Sec. III we consider the Hubbard ladder at small dopings. In Sec. IV we present our results for the ground state energies and compare with DMRG. Finally, in Sec. V we summarize our results and present some concluding remarks.

II. HALF-FILLED HUBBARD LADDER

We begin with the half-filled ladder. What are the ingredients necessary to construct a wave function which captures the physics of the half-filled Hubbard ladder? A trail of clues has been laid by previous works. First of all, we know that at strong coupling the half-filled

$$|\Psi_0\rangle = \boxed{\square} + a_1 \boxed{\square} + a_2 \left(\boxed{\square} + \boxed{\square} \right) + a_3 \left(\boxed{\square} + \boxed{\square} \right) + a_4 \left(\boxed{\square} + \boxed{\square} + \boxed{\square} + \boxed{\square} \right) + a_5 \left(\boxed{\square} + \boxed{\square} + \boxed{\square} + \boxed{\square} \right)$$

FIG. 1. Ground state wave function for the 2×2 half-filled plaquette. A circled link represents a singlet bond. (See text for a full explanation of each state.)

Hubbard model is equivalent to the Heisenberg model. Secondly, it is known that the two-leg Heisenberg ladder (and Hubbard ladder) have a spin gap and short range spin correlations. Furthermore, it has been shown that the resonating valence bond (RVB) state captures the essential physics of the two-leg Heisenberg ladder.^{12,8} Hence, the RVB picture should capture the essential physics of the half-filled Hubbard ladder at strong coupling. Thus we propose a generalization of the RVB state as our variational ansatz.

A key property of the RVB state is that it is the exact solution to the 2×2 Heisenberg plaquette. Therefore, we base our generalized RVB state on the exact solution to the 2×2 Hubbard plaquette. Since the 2×2 plaquette will serve as the basis for our ansatz, we discuss it in detail below.

A. The 2×2 Plaquette

The ground state of the 2×2 plaquette is given by

$$|\psi_0\rangle = |\varphi_0\rangle + a_1 |\varphi_1\rangle + a_2 |\varphi_2\rangle + a_3 |\varphi_3\rangle + a_4 |\varphi_4\rangle + a_5 |\varphi_5\rangle \quad (4)$$

where

$$\begin{aligned} |\varphi_0\rangle &= \Delta_{(1,1),(1,2)}^\dagger \Delta_{(2,1),(2,2)}^\dagger |0\rangle, \\ |\varphi_1\rangle &= \Delta_{(1,1),(2,1)}^\dagger \Delta_{(1,2),(2,2)}^\dagger |0\rangle, \\ |\varphi_2\rangle &= D_{(1,1)}^\dagger D_{(1,2)}^\dagger |0\rangle + D_{(2,1)}^\dagger D_{(2,2)}^\dagger |0\rangle, \\ |\varphi_3\rangle &= D_{(1,1)}^\dagger D_{(2,1)}^\dagger |0\rangle + D_{(1,2)}^\dagger D_{(2,2)}^\dagger |0\rangle, \\ |\varphi_4\rangle &= \Delta_{(1,1),(1,2)}^\dagger D_{(2,1)}^\dagger |0\rangle + \Delta_{(1,1),(1,2)}^\dagger D_{(2,2)}^\dagger |0\rangle \\ &\quad + \Delta_{(2,1),(2,2)}^\dagger D_{(1,1)}^\dagger |0\rangle + \Delta_{(2,1),(2,2)}^\dagger D_{(1,2)}^\dagger |0\rangle, \\ |\varphi_5\rangle &= \Delta_{(1,1),(2,1)}^\dagger D_{(1,2)}^\dagger |0\rangle + \Delta_{(1,1),(2,1)}^\dagger D_{(2,2)}^\dagger |0\rangle \\ &\quad + \Delta_{(1,2),(2,2)}^\dagger D_{(1,1)}^\dagger |0\rangle + \Delta_{(1,2),(2,2)}^\dagger D_{(2,1)}^\dagger |0\rangle. \end{aligned} \quad (5)$$

$|\psi_0\rangle$ is shown schematically in Fig. 1.

We will be mainly interested in the case $t = t_\perp$. In Table I we list the values of the parameters for several values of U (with $t = t_\perp = 1$).

$$(a) \left(\boxed{\square} + \boxed{\square} \right) \quad (b) \left(\boxed{\square} + \boxed{\square} + \boxed{\square} + \boxed{\square} \right)$$

FIG. 2. States which the B_2 representation prevents from appearing in the ground state wave function of the half-filled plaquette.

TABLE I. Values of the parameters for the half-filled 2×2 plaquette (with $t = t_\perp = 1$) which give the exact groundstate.

U	a_1	a_3	a_5	a_2	a_4
8	-1.0	-0.0762	-0.3306	$-a_3$	$-a_5$
16	-1.0	-0.0221	-0.1807	$-a_3$	$-a_5$
24	-1.0	-0.0101	-0.1229	$-a_3$	$-a_5$

Notice that the solution to the 2×2 plaquette (with $t = t_\perp$) has D_4 symmetry. (D_4 is the symmetry group of the square.) However, the ground state does *not* transform in the scalar representation of D_4 ; it transforms in the B_2 representation of D_4 . (B_2 is the one-dimensional representation which changes sign upon rotation by 90° and reflection about the diagonals.) B_2 coincides with the standard $d_{x^2-y^2}$ symmetry. The B_2 representation is what forbids some configurations, as those shown in Fig. 2, from appearing in the ground state wave function.

A few more words are in order about the ground state wave function. Notice that $a_1 = -1$ (i.e., the weight of the horizontal singlets is equal to (minus) the weight of the vertical singlets.) This is the RVB mechanism – the system lowers its energy by resonating between horizontal and vertical singlets; a_1 is the “RVB parameter”. Also, notice that $|a_2|, |a_3| = \mathcal{O}(a_4^2)$. This will play a role in constructing the Ansatz for the half-filled ladder.

B. The Ladder

Using the configurations of the 2×2 plaquette as the basis of our Ansatz for the ladder, a typical configuration for the ladder is shown in Fig. 3. The ground state will be a superposition of all possible configurations of the type shown in Fig. 3. Therefore, it seems like working with this kind of state will be a formidable task. Fortunately, the RVA gives us a straightforward way of dealing with such a state – generate it *recursively*. Specifically, the RVA builds the ground state of a ladder with $N + \nu$ rungs using the knowledge of the ground states of a ladder with $N, N + 1, \dots, N + \nu - 1$ rungs. This is achieved by recursion relations which express the ground state $|N + \nu\rangle$ in terms of the ground states $\{|N + i\rangle\}$ with $i = 0, \dots, \nu - 1$.⁸

Using these ingredients, we consider the following ansatz for the half-filled Hubbard ladder which is shown

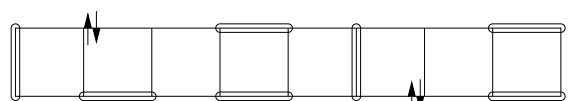


FIG. 3. Typical configuration appearing in the ground state wave function of the half-filled ladder.

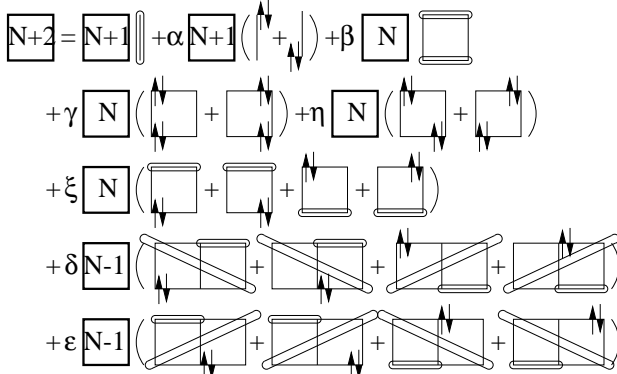


FIG. 4. The RVA ansatz for the half-filled Hubbard ladder. Note that links or sites connected with a circle represent a singlet bond.

$$\begin{aligned}
|N+2\rangle = & |\phi_0\rangle_{N+2} |N+1\rangle + \alpha |\phi_1\rangle_{N+2} |N+1\rangle \\
& + \beta |\phi_2\rangle_{N+1,N+2} |N\rangle + \gamma |\phi_3\rangle_{N+1,N+2} |N\rangle \\
& + \xi |\phi_4\rangle_{N+1,N+2} |N\rangle + \eta |\phi_5\rangle_{N+1,N+2} |N\rangle \\
& + \delta |\phi_6\rangle_{N,N+1,N+2} |N-1\rangle \\
& + \epsilon |\phi_7\rangle_{N,N+1,N+2} |N-1\rangle
\end{aligned} \quad (6)$$

schematically in Fig. 4.¹³ For completeness, the states in terms of the operators in Eqs. 2 and 3 are given in Appendix A.

A few words are in order about the configurations in our Ansatz. i) β , the weight of the horizontal bond (relative to the vertical bond), is the “RVB parameter”. For a true RVB state, we would have $\beta = -1$. Although we do not expect $\beta = -1$, from work on the Heisenberg model the variational parameters were shown to evolve smoothly with system size;⁸ we expect $|\beta| = \mathcal{O}(1)$. ii) Suppose we iterate the recursion relations once. Then $|\phi_0\rangle$ and $|\phi_1\rangle$ (and also $|\phi_5\rangle$) generate the terms shown in Fig. 5. In the ground state of the 2x2 plaquette, the states in Fig. 5(b) have weight $\mathcal{O}(\alpha)$, the states in Fig. 5(c) have weight $\mathcal{O}(\alpha^2)$, and the states in Fig. 5(d) do not appear. Since we expect the parameters to evolve smoothly,⁸ we expect $\eta \approx -\alpha^2$. (η is behaving as a “counter-term”; it’s job is to subtract off the α^2 contribution from $|\phi_1\rangle$.) iii) Even though we no longer have D_4 symmetry, initial calculations showed that the states in Fig. 2(b) do not appear in the ground state of the Hubbard ladder. (This is another indication that the parameters evolve smoothly from the 2x2 case to the ladder.) Therefore, we do not consider them in what follows. iv) Since the configurations $|\phi_6\rangle_{N,N+1,N+2}$ and $|\phi_7\rangle_{N,N+1,N+2}$ appear as intermediate states for the

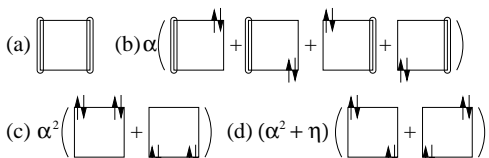


FIG. 5. States generated by $|\phi_0\rangle$ and $|\phi_1\rangle$ (and also $|\phi_5\rangle$) by running the recursion relations once.

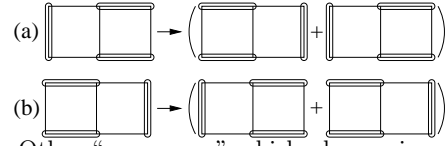


FIG. 6. Other “resonances” which play an important role in the RVB picture.

resonances shown in Fig. 6, it is necessary to include these states in the Ansatz to give us an RVB state. This can easily be seen by comparing the weights of the coefficients as shown in Table II (see below).

In order to compute the values of the coefficients, we treat them as variational parameters and minimize the ground state energy with respect to these parameters. The ground state energy and other quantities appear as recursion relations. It will be useful to define

$$\begin{aligned}
E_N &= \langle N | H_N | N \rangle, \\
D_N &= \langle N-1 |_N \langle \phi_0 | H_N | N \rangle, \\
C_N &= \langle N-1 |_N \langle \phi_1 | H_N | N \rangle, \\
Z_N &= \langle N | N \rangle, \\
Y_N &= \langle N-1 |_N \langle \phi_0 | N \rangle, \\
X_N &= \langle N-1 |_N \langle \phi_1 | N \rangle.
\end{aligned} \quad (7)$$

They are supplemented by the initial conditions

$$\begin{aligned}
Z_0 &= 1, Y_0 = 0, X_0 = 0, \\
E_0 &= 0, D_0 = 0, C_0 = 0.
\end{aligned} \quad (8)$$

To determine the values for the variational parameters for a given (finite) value of N , we iterate the recursion relations and minimize the quantity E_N/Z_N numerically. The actual recursion relations are quite unwieldy; we have relegated them, as well as their derivation, to Appendix A.

The values of the variational parameters for various values of U (with $t = t_\perp = 1$) are shown in Table II. The results were obtained on a 2×32 ladder. Notice that i) $|\beta| = \mathcal{O}(1)$, and we have produced an RVB state. ii) $|\eta| = \mathcal{O}(\alpha^2)$, and η is indeed behaving as a counterterm. iii) $|\delta|, |\epsilon| \approx \alpha/3$. Therefore, these configurations are non-negligible, suggesting that the resonances shown in Fig. 6 are important to the RVB picture.

III. THE DOPED HUBBARD LADDER

Now, we consider the doped Hubbard ladder. In Ref. 9 it was shown that hole pairs moving through an RVB

TABLE II. Values of the variational parameters for a 2×32 half-filled ladder with $t = t_\perp = 1$.

U	α	β	γ	ξ	η	δ	ϵ
8	.3296	-.8710	-.0782	-.2877	-.0938	.1031	.1031
16	.1848	-.8800	-.0243	-.1606	-.0299	.0639	.0639
24	.1265	-.8817	-.0113	-.1097	-.0142	.0451	.0451

$$|\Psi_0\rangle = \left(\begin{array}{c} \square \\ \square \end{array} + \begin{array}{c} \square \\ \square \end{array} \right) + b_1 \left(\begin{array}{c} \square \\ \square \end{array} + \begin{array}{c} \square \\ \square \end{array} \right) + b_2 \left(\begin{array}{c} \square \\ \square \end{array} + \begin{array}{c} \square \\ \square \end{array} \right) + b_3 \left(\begin{array}{c} \square \\ \square \end{array} + \begin{array}{c} \square \\ \square \end{array} + \begin{array}{c} \square \\ \square \end{array} + \begin{array}{c} \square \\ \square \end{array} \right)$$

FIG. 7. Ground state wave function for the 2×2 plaquette with two holes.

background captures the essential physics of the $t - J$ ladder at small dopings. Since the $t - J$ model is the large U limit of the Hubbard model, we expect this picture to hold for the Hubbard model at large U and small dopings. Therefore, we consider an Ansatz of hole pairs moving through our generalized RVB background for the Hubbard ladder at small dopings.

Since the structure of the hole pairs is based on the exact solution to the 2×2 plaquette with 2 holes, we consider the 2×2 case in detail below.

A. The 2×2 Plaquette with Two Holes

The ground state of the 2×2 plaquette with 2 holes is given by

$$|\psi_0^h\rangle = |\varphi_0^h\rangle + b_1 |\varphi_1^h\rangle + b_2 |\varphi_2^h\rangle + b_3 |\varphi_3^h\rangle \quad (9)$$

where

$$\begin{aligned} |\varphi_0^h\rangle &= \Delta_{(1,1),(1,2)}^\dagger |0\rangle + \Delta_{(2,1),(2,2)}^\dagger |0\rangle, \\ |\varphi_1^h\rangle &= \Delta_{(1,1),(2,1)}^\dagger |0\rangle + \Delta_{(1,2),(2,2)}^\dagger |0\rangle, \\ |\varphi_2^h\rangle &= \Delta_{(1,1),(2,2)}^\dagger |0\rangle + \Delta_{(2,1),(1,2)}^\dagger |0\rangle, \\ |\varphi_3^h\rangle &= D_{(1,1)}^\dagger |0\rangle + D_{(1,2)}^\dagger |0\rangle \\ &\quad + D_{(2,1)}^\dagger |0\rangle + D_{(2,2)}^\dagger |0\rangle. \end{aligned} \quad (10)$$

$|\psi_0^h\rangle$ is shown schematically in Fig. 7.

In Table III we list the values of the parameters for several values of U (with $t = t_\perp = 1$).

Notice that the solution to the 2×2 case (with $t = t_\perp$) has D_4 symmetry. However, now the ground state transforms in the *scalar* representation of D_4 . Recalling

TABLE III. Values of the parameters for the 2×2 plaquette with two holes (with $t = t_\perp = 1$) which gives the exact ground state.

U	b_1	b_2	b_3
8	1.0	1.2470	0.3569
16	1.0	1.3131	0.2100
24	1.0	1.3420	0.1483

that the ground state of the half-filled ladder transforms in the B_2 representation, we see that the operator that creates a hole pair out of the undoped system has $d_{x^2-y^2}$ symmetry.¹⁴ These facts continue to be true for low doping in larger ladders. Also, notice that $b_3 = \mathcal{O}(\alpha)$ where α is from the half-filled ladder. This will play a role in writing our Ansatz for the doped ladder.

B. The Ladder

Using the configurations of the generalized RVB state as well as the hole pair configurations, a typical configuration for the doped ladder is shown in Fig. 8.

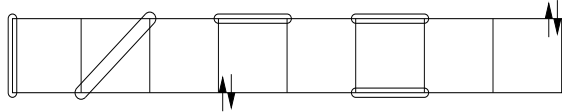


FIG. 8. Typical configuration appearing in the ground state wave function of the doped ladder.

The ground state will be a superposition of all such configurations shown in Fig. 8. Fortunately, we can generate such a state *recursively*. Specifically, we build the ground state of a ladder with $N + \nu$ rungs and $P + \mu$ holes using the knowledge of the ground states of a ladder with $N, N + 1, \dots, N + \nu - 1$ rungs and $P, P + 1, \dots, P + \mu$ holes. This is achieved by recursion relations which express the ground state $|N + \nu, P + \mu\rangle$ in terms of the ground states $\{|N + i, P + j\rangle\}$ with $i = 0, \dots, \nu - 1$ and $j = 0, \dots, \mu$.⁹

Using the above ingredients, we consider the following Ansatz for the doped Hubbard ladder

$$\begin{aligned} |N + 2 P + 1\rangle &= |\phi_0\rangle_{N+2} |N + 1 P + 1\rangle + \alpha |\phi_1\rangle_{N+2} |N + 1 P + 1\rangle + \beta |\phi_2\rangle_{N+1,N+2} |N P + 1\rangle \\ &\quad + \gamma |\phi_3\rangle_{N+1,N+2} |N P + 1\rangle + \xi |\phi_4\rangle_{N+1,N+2} |N P + 1\rangle + \eta |\phi_5\rangle_{N+1,N+2} |N P + 1\rangle \\ &\quad + \delta |\phi_6\rangle_{N,N+1,N+2} |N - 1 P + 1\rangle + \varepsilon |\phi_7\rangle_{N,N+1,N+2} |N - 1 P + 1\rangle \\ &\quad + |\phi_0^h\rangle_{N+2} |N + 1 P\rangle + \lambda |\phi_1^h\rangle_{N+1,N+2} |N P\rangle + \zeta |\phi_2^h\rangle_{N+1,N+2} |N P\rangle \\ &\quad + \mu |\phi_3^h\rangle_{N,N+1,N+2} |N - 1 P\rangle + \nu |\phi_4^h\rangle_{N,N+1,N+2} |N - 1 P\rangle \end{aligned} \quad (11)$$

FIG. 9. The RVA Ansatz for the doped Hubbard ladder.

which is shown schematically in Fig. 9. For completeness, the states in terms of the operators in Eqs. 2 and 3 are given in Appendix B.

A few words are in order about the configurations in our Ansatz. i) The Ansatz contains the configurations for the RVB state, as well as the configurations for holes bound in pairs. The hole pair states are based on the exact solution to the 2×2 plaquette with 2 holes, and our ansatz reproduces this exact solution. ii) The states $|\phi_3^h\rangle_{N,N+1,N+2}$ and $|\phi_4^h\rangle_{N,N+1,N+2}$ extend over three rungs. These states are necessary to allow the hole pairs to move smoothly through the RVB background. iii) Note that physically, the picture of hole pairs moving through an RVB background can only be appropriate for low dopings.

To compute the values of the coefficients in our Ansatz, we treat them as variational parameters and minimize the ground-state energy with respect to these parameters. It will be useful to define

$$\begin{aligned}
 E_{N,P} &= \langle N P | H_N | N P \rangle, \\
 D_{N,P} &= \langle N-1 P |_N \langle \phi_0 | H_N | N P \rangle, \\
 C_{N,P} &= \langle N-1 P |_N \langle \phi_1 | H_N | N P \rangle, \\
 Z_{N,P} &= \langle N P | N P \rangle, \\
 Y_{N,P} &= \langle N-1 P |_N \langle \phi_0 | N P \rangle, \\
 X_{N,P} &= \langle N-1 P |_N \langle \phi_1 | N P \rangle. \quad (12)
 \end{aligned}$$

They are supplemented by the initial conditions

$$\begin{aligned}
 Z_{N,P=N} &= 1, Y_{N,P=N} = 0, X_{N,P=N} = 0, \\
 E_{N,P=N} &= 0, D_{N,P=N} = 0, C_{N,P=N} = 0, \\
 F_{N < P,P} &= 0 \text{ for } F = Z, Y, X, E, D, C. \quad (13)
 \end{aligned}$$

To determine the values for the variational parameters

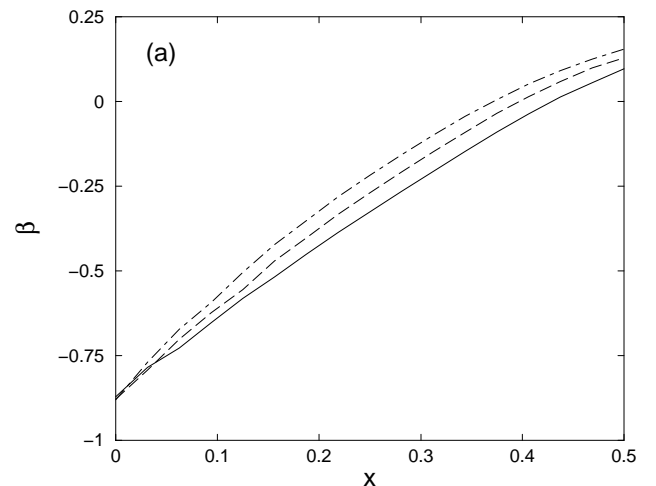
for given (finite) values of N and P , we iterate the recursion relations and we minimize the quantity $E_{N,P}/Z_{N,P}$. The actual recursion relations are quite unwieldy; we have relegated them, as well as their derivation, to Appendix B.

What is the nature of the state we have constructed? In order to answer this question, we plot β , λ , and ζ vs. doping. These parameters contain most of the physics of our Ansatz. β is the “RVB parameter”; λ and ζ are the weights of the hole pair configurations. The results were obtained on a 2×32 ladder.

First, consider Fig. 10(a). β begins at $\mathcal{O}(-1)$ and increases (i.e., becomes less negative) with doping until a critical doping, x_c , where it vanishes. Beyond this doping, β is positive. This has also been found for the $t-J$ ladder.⁹ Upon doping, the hole pairs cause destructive interference which degrades the RVB mechanism. For $x > x_c$, this destructive interference has driven β positive, and it is no longer appropriate to think of our state as describing hole pairs moving through an RVB background.⁹

Similar to the $t-J$ ladder, the difference between $x < x_c$ and $x > x_c$ can be attributed to two different internal structures of the hole pairs. For $x < x_c$ the hole pairs have a $d_{x^2-y^2}$ structure relative to the RVB background. For $x > x_c$ the hole pairs have an s -wave like symmetry relative to their background.⁹

Now consider Figs. 10(b) and 10(c). First of all, notice that $\lambda > \zeta$. This shows the importance of the diagonal frustrating bonds for all dopings.¹⁵ Also, notice that λ and ζ both reach their maximum at $x = 1/2$. At $x = 1/2$ the system is essentially a large scale reproduction of the 2×2 plaquette with 2 holes.⁹ Indeed, the values of λ and ζ at $x = 1/2$ are similar to their values for the 2×2 plaquette.



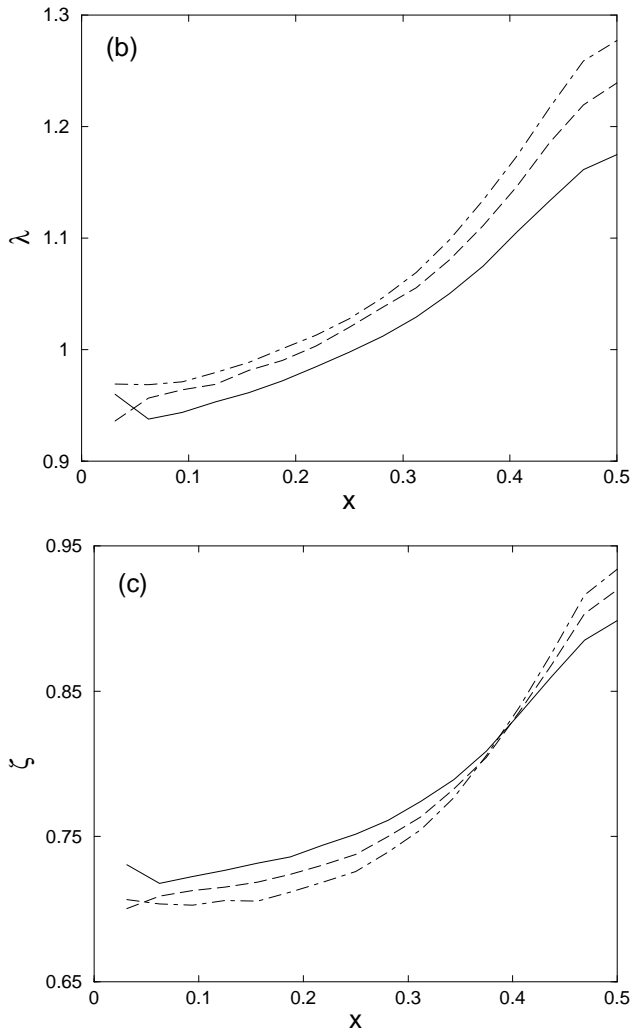


FIG. 10. (a) β vs. doping, x , for a 2×32 ladder at $U=8$ (solid line), $U=12$ (dashed line), and $U=16$ (dashed-dotted line). (b) Same as (a) for λ . (c) Same as (a) for ζ .

IV. GROUND STATE ENERGIES

First, we show results for Energy per site vs. U in Fig. 11. For comparison, DMRG results are presented for the same set of parameters.¹⁶ At half-filling, as we would expect, our Ansatz is most accurate for large U and large t_{\perp} . The ground state energy per site for a 2×32 half-filled ladder as a function of U for various t_{\perp} is shown in Fig. 11(a). For $U = 8$ and $t_{\perp} = 1$, the energy from the RVA agrees with DMRG to within 90% and improves as U or t_{\perp} is increased. Up to about $U = 10$, longer bonds (extending over at least 3 rungs) are coming into play. These states should be included in the Ansatz to further improve the overlap with the ground state. At $U = 16$ and $t_{\perp} = 1$, our ansatz gives a ground state energy within 94% of the DMRG result.

It should be noted that for the Heisenberg ladder, the RVB state gives a ground state energy within 94% of true

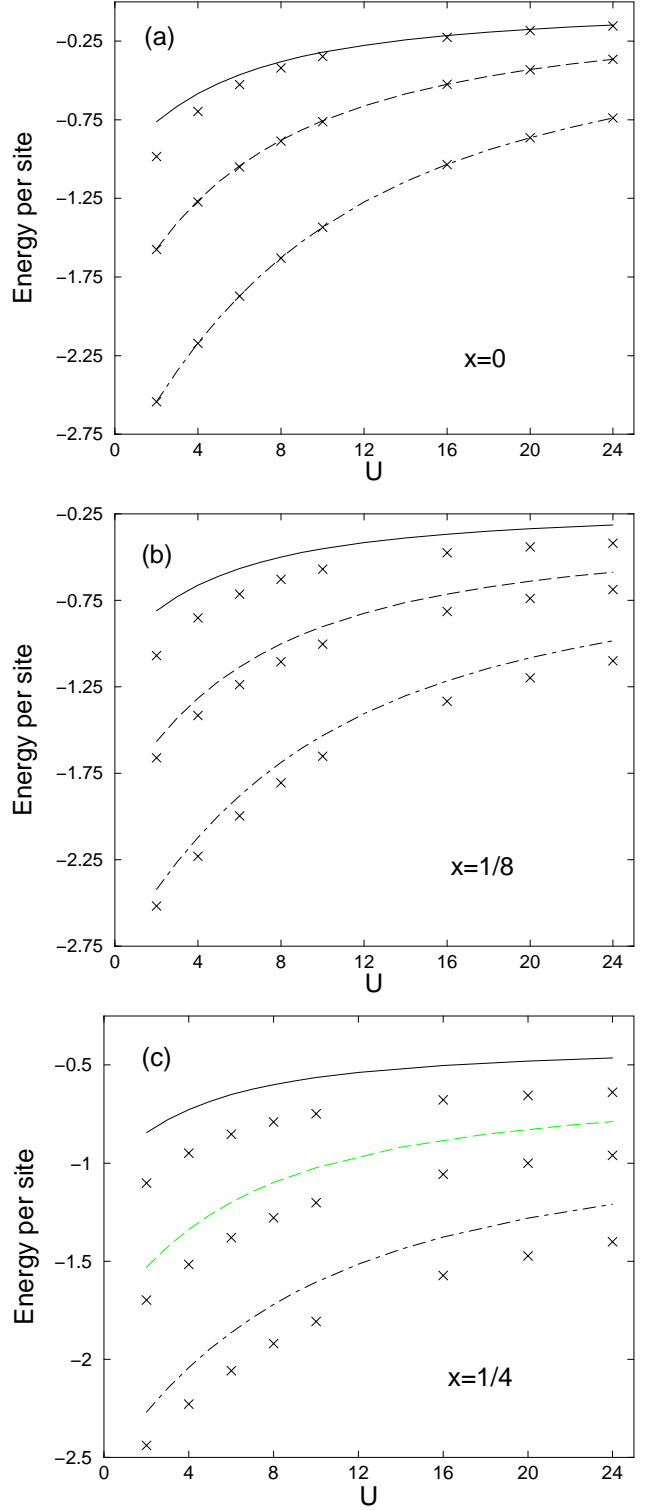


FIG. 11. (a) Ground state energy per site at half-filling ($x = 0$) vs. U for $t_{\perp} = 1$ (solid line), $t_{\perp} = 2$ (dashed line), $t_{\perp} = 3$ (dashed-dotted line). For comparison, DMRG results (shown as \times) are presented for the same set of parameters. (b) Same as (a) except for $x = 1/8$. (c) Same as (a) except for $x = 1/4$.

ground state energy, obtained from DMRG.⁸ A recent

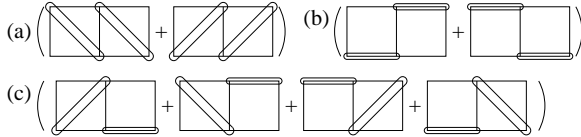


FIG. 12. “Pair-breaking” configurations which are playing a rather large role in the ground state of the doped Hubbard ladder.

DMRG study of different ladder models found that the Hubbard model and Heisenberg model begin to agree only for rather large U ($U \approx 16$).¹⁷ Therefore, it is not surprising that the RVB picture becomes as good for the Hubbard model as it is for the Heisenberg model at $U \approx 16$.

Fig. 11(b) shows the ground state energy of the RVA Ansatz as a function of U for various t_{\perp} for a doping of $x = 1/8$ on a 2×32 ladder. Again, we show energies obtained from DMRG for the same set of parameters. For $U = 16$ and $t_{\perp} = 1$, the two energies agree to only within 77% and improves slightly as t_{\perp} is increased. For example, at $U = 16$ and $t_{\perp} = 2$, the overlap of energies increases to 87%. Further discrepancies occur when the doping is increased to $x = 1/4$ (see Fig. 11(c)).

The differences in ground state energies occur due to the importance of “pair-breaking” configurations, like those shown in Fig. 12. The weights of these types of states increase as we move away from half-filling. Consequently, to further improve the RVA Ansatz, such states must be included in the wave function. Note also that our Ansatz would be essentially exact for the case where hole pairs are well localized on a rung. For the $t - J$ model with $J_{\text{rung}} \gg J_{\text{chain}}, t$, pairs are well localized along a rung, and the ground state is essentially a product of rung singlets and rung hole pairs. However, for the Hubbard model at strong coupling (i.e., $U \gg t_{\perp}, t$), this is not the case. Holes would always rather occupy adjacent rungs, even for $t_{\perp} \gg t$, since this minimizes the Coulomb energy from doubly occupied sites. To see this consider a 2×2 plaquette with 2 holes; let $t \ll t_{\perp}$ and $t, t_{\perp} \ll U$. With 1 particle on each rung (i.e., one hole on each rung), the ground state energy is approximately $-2t_{\perp}$; with both particles on the same rung (i.e., both holes on the same rung), the ground state energy is approximately $-J = -4t_{\perp}^2/U$. Therefore, at large U , the particles would rather occupy adjacent rungs. (See Fig. 13.)

The situation we have with the doped ladder is similar to what we had for the half-filled ladder in the early stages of this work. We found that without the states

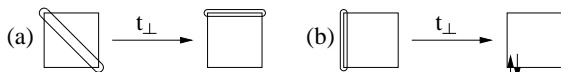


FIG. 13. For $t \ll t_{\perp}$, hopping along the rung dominates. By putting the particles (or holes) on adjacent rungs, we can have the situation shown in (a). However, by putting both particles (or holes) on the same rung, we get the situation shown in (b), which is energetically unfavorable.

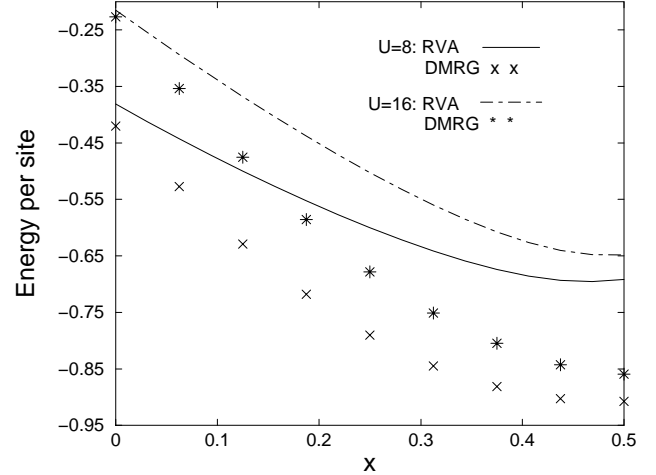


FIG. 14. Ground state energy per site vs. doping for a 2×32 ladder (with $t = t_{\perp} = 1$) for $U = 8$ (solid line) and $U = 16$ (dashed-dotted line). For comparison, DMRG results for $U = 8$ (\times) and $U = 16$ ($*$) are shown.

$|\phi_6\rangle$ and $|\phi_7\rangle$ which extend over three rungs (see Fig. 4), the RVA did not accurately reproduce the ground state even at extremely large U . However, once we included $|\phi_6\rangle$ and $|\phi_7\rangle$, the results from the RVA improved drastically. Based on these results, we expect the RVA to greatly improve by including the states shown in Fig. 12.

In Fig. 14 we plot Energy per site vs. Doping for a 2×32 ladder for $U = 8$ and $U = 16$ (with $t_{\perp} = 1$) in order to better understand the region of validity of our RVA ansatz. Again, we see good agreement with DMRG results at half-filling. However, as soon as we dope, configurations like those shown in Fig. 12 are also important.

It is interesting to note that the idea of hole pairs moving through the RVB background seems to more accurately represent the ground state of the $t - J$ model than the Hubbard model. Using the well known relation at strong coupling, $J \approx \frac{4t^2}{U}$, the RVA agrees to within 92% of the true ground state energy of the $t - J$ ladder for $J = 0.5$ ($U = 8$) at a doping of $x = 1/8$. There are two ways to interpret this; either the $t - J$ model supports pairing better than the Hubbard model, or we must view the hole pairs in the Hubbard model as having a larger size (i.e. larger coherence length.)

V. CONCLUDING REMARKS

To summarize, we applied the Recurrent Variational Approach to the two-leg Hubbard ladder. Our results were in qualitative agreement with previous results on the Heisenberg and $t - J$ ladders. For the half-filled ladder, the generalized RVB state became more accurate in the parameter regime where the Hubbard and Heisenberg ladders were shown to coincide. However, comparison of the RVA with DMRG for the doped ladder indicate that hole-pairs moving through an RVB background

is incomplete; it does not capture the essential physics. “Pair-breaking” configurations are also necessary to capture the essential physics.

As we saw, the strength of the RVA is the ease in which we could extract the physics. We were able to see the importance of the configurations in our Ansatz quite easily. Furthermore, the RVA has a natural way in which to include longer bonds in the Ansatz to more accurately represent the groundstate wavefunction. The importance of such additional states to the physics of the ladder is not easily probed with other techniques.

Generalized RVB states similar to ours have been considered previously for the half-filled Hubbard ladder.¹⁸ Fano *et. al.* were even able to produce an Ansatz coming within 98% of the true groundstate energy for a (half-filled) 2x4 ladder at $U = 16$. (Their Ansatz included diagonal bonds of length $\sqrt{5}$.) However, none of these works considered the doped case. Using the approach in Ref. 17 (in terms of dimer coverings), it appears to be a formidable task to consider doping. This is one of the strengths of the RVA; doping is handled rather easily. Even though our results for the doped ladder showed that hole pairs moving through an RVB background is incomplete, the RVA offers a straightforward way to improve the situation, namely include “pair-breaking” configurations (shown in Fig. 12) in the Ansatz.

Another (and probably better) way to improve the situation for the doped ladder is to consider a Matrix Product Ansatz.^{19,20} A Matrix Product Ansatz can be gen-

erated by first order recursion relations.²⁰ In the RVA, the size of the hole-pairs are fixed. (In our case, the hole pairs had a size of one lattice spacing.) However, by construction, the Matrix Product Ansatz takes into account hole pairs of *arbitrary* size. We leave this (and other possibilities) for future work.

ACKNOWLEDGMENTS

We would like to thank D. J. Scalapino, S. Daul, S. Hortikar, R. Konik, C. L. Martin, and M. A. Martin-Delgado for helpful discussions and comments. EHK gratefully acknowledges the warm hospitality of Argonne National Laboratory where parts of this manuscript were written. DD would like to thank S. Daul and R. M. Noack for assistance with the DMRG results presented here. EHK was supported by NSF grant No. DMR-9527304, GS by DGES grant PB97-1190, and DD by DOE grant No. DE-FG03-85ER451907.

APPENDIX A: THE HALF-FILLED LADDER

The states in the Ansatz for the half-filled ladder of Eq. 6 are given by

$$\begin{aligned}
|\phi_0\rangle_{N+2} &= \Delta_{(N+2,1),(N+2,2)}^\dagger |0\rangle_{N+2}, \\
|\phi_1\rangle_{N+2} &= D_{(N+2,1)}^\dagger |0\rangle_{N+2} + D_{(N+2,2)}^\dagger |0\rangle_{N+2}, \\
|\phi_2\rangle_{N+1,N+2} &= \Delta_{(N+1,1),(N+2,1)}^\dagger \Delta_{(N+1,2),(N+2,2)}^\dagger |0\rangle_{N+1,N+2}, \\
|\phi_3\rangle_{N+1,N+2} &= D_{(N+1,1)}^\dagger D_{(N+1,2)}^\dagger |0\rangle_{N+1,N+2} + D_{(N+2,1)}^\dagger D_{(N+2,2)}^\dagger |0\rangle_{N+1,N+2}, \\
|\phi_4\rangle_{N+1,N+2} &= \Delta_{(N+1,1),(N+2,1)}^\dagger D_{(N+1,2)}^\dagger |0\rangle_{N+1,N+2} + \Delta_{(N+1,1),(N+2,1)}^\dagger D_{(N+2,2)}^\dagger |0\rangle_{N+1,N+2} \\
&\quad + \Delta_{(N+1,2),(N+2,2)}^\dagger D_{(N+1,1)}^\dagger |0\rangle_{N+1,N+2} + \Delta_{(N+1,2),(N+2,2)}^\dagger D_{(N+2,1)}^\dagger |0\rangle_{N+1,N+2}, \\
|\phi_5\rangle_{N+1,N+2} &= D_{(N+1,1)}^\dagger D_{(N+2,2)}^\dagger |0\rangle_{N+1,N+2} + D_{(N+1,2)}^\dagger D_{(N+2,1)}^\dagger |0\rangle_{N+1,N+2}, \\
|\phi_6\rangle_{N,N+1,N+2} &= \Delta_{(N,1),(N+2,2)}^\dagger \Delta_{(N+1,1),(N+2,1)}^\dagger D_{(N,2)}^\dagger |0\rangle_{N,N+1,N+2} \\
&\quad + \Delta_{(N,1),(N+2,2)}^\dagger \Delta_{(N+1,1),(N+2,1)}^\dagger D_{(N+1,2)}^\dagger |0\rangle_{N,N+1,N+2} \\
&\quad + \Delta_{(N,2),(N+2,1)}^\dagger \Delta_{(N+1,2),(N+2,2)}^\dagger D_{(N,1)}^\dagger |0\rangle_{N,N+1,N+2} \\
&\quad + \Delta_{(N,2),(N+2,1)}^\dagger \Delta_{(N+1,2),(N+2,2)}^\dagger D_{(N+1,1)}^\dagger |0\rangle_{N,N+1,N+2}, \\
|\phi_7\rangle_{N,N+1,N+2} &= \Delta_{(N,1),(N+2,2)}^\dagger \Delta_{(N,2),(N+1,2)}^\dagger D_{(N+1,1)}^\dagger |0\rangle_{N,N+1,N+2} \\
&\quad + \Delta_{(N,1),(N+2,2)}^\dagger \Delta_{(N,2),(N+1,2)}^\dagger D_{(N+2,1)}^\dagger |0\rangle_{N,N+1,N+2} \\
&\quad + \Delta_{(N,2),(N+2,1)}^\dagger \Delta_{(N,1),(N+1,1)}^\dagger D_{(N+1,2)}^\dagger |0\rangle_{N,N+1,N+2} \\
&\quad + \Delta_{(N,2),(N+2,1)}^\dagger \Delta_{(N,1),(N+1,1)}^\dagger D_{(N+2,2)}^\dagger |0\rangle_{N,N+1,N+2}. \tag{1}
\end{aligned}$$

To derive the recursion relations, the following inner products are necessary:

$$\begin{aligned}
&_{N+2}\langle\phi_0|\phi_0\rangle_{N+2}=2, \quad _{N+2}\langle\phi_1|\phi_1\rangle_{N+2}=2, \quad _{N+1,N+2}\langle\phi_2|\phi_2\rangle_{N+1,N+2}=4, \\
&_{N+1,N+2}\langle\phi_3|\phi_3\rangle_{N+1,N+2}=2, \quad _{N+1,N+2}\langle\phi_4|\phi_4\rangle_{N+1,N+2}=8, \quad _{N+1,N+2}\langle\phi_5|\phi_5\rangle_{N+1,N+2}=2, \\
&_{N,N+1,N+2}\langle\phi_6|\phi_6\rangle_{N,N+1,N+2}=16, \quad _{N,N+1,N+2}\langle\phi_7|\phi_7\rangle_{N,N+1,N+2}=16, \\
&\langle N+1|_{N+2}\langle\phi_0|\phi_2\rangle_{N+1,N+2}|N\rangle=(-1)\langle N+1|\phi_0\rangle_{N+1}|N\rangle, \\
&\langle N+1|_{N+2}\langle\phi_1|\phi_5\rangle_{N+1,N+2}|N\rangle=\langle N+1|\phi_1\rangle_{N+1}|N\rangle, \\
&\langle N+1|_{N+2}\langle\phi_0|\phi_6\rangle_{N,N+1,N+2}|N-1\rangle=(-1)\langle N+1|\phi_4\rangle_{N,N+1}|N-1\rangle, \\
&\langle N|_{N+1,N+2}\langle\phi_4|\phi_7\rangle_{N,N+1,N+2}|N-1\rangle=(-4)\langle N|\phi_0\rangle_N|N-1\rangle. \tag{2}
\end{aligned}$$

Using these inner products, a straightforward calculation gives the following (coupled) recursion relations:

$$\begin{aligned}
Z_{N+2} &= (2+2\alpha^2)Z_{N+1} - 2\beta Y_{N+1} + 2\alpha\eta X_{N+1} + (4\beta^2 + 2\gamma^2 + 8\xi^2 + 2\eta^2)Z_N \\
&\quad + (16\delta^2 + 16\varepsilon^2 - 16\xi\delta)Z_{N-1} - 8\xi\varepsilon Y_N + 8\delta\varepsilon Y_{N-1}, \\
Y_{N+2} &= 2Z_{N+1} - \beta Y_{N+1} - 8\xi\delta Z_{N-1} + 4\delta\varepsilon Y_{N-1}, \\
X_{N+2} &= 2\alpha Z_{N+1} + \eta X_{N+1}, \\
E_{N+2} &= (2+2\alpha^2)E_{N+1} + (-8t_\perp\alpha + 2U\alpha^2)Z_{N+1} - 2\beta D_{N+1} + 2\alpha\eta C_{N+1} \\
&\quad + (8t\xi + 4t_\perp\alpha\beta)Y_{N+1} + (-4t_\perp\eta - 8t\alpha\xi + 2U\alpha\eta)X_{N+1} \\
&\quad + (4\beta^2 + 2\gamma^2 + 8\xi^2 + 2\eta^2)E_N + (-32t\beta\xi + 4U\gamma^2 - 16t\gamma\xi + 8U\xi^2 - 16t\xi\eta + 4U\eta^2)Z_N \\
&\quad + (16t\beta\delta - 8t\varepsilon + 8t\alpha^2\varepsilon + 16t\beta\varepsilon + 8t\gamma\varepsilon - 8U\xi\varepsilon + 8t\eta\varepsilon - 8t\delta)Y_N + 8t\alpha\delta X_N \\
&\quad + (32t\beta\varepsilon + 16U\delta^2 + 16U\varepsilon^2 + 32t\beta\delta + 16t\gamma\delta - 16U\xi\delta + 16t\eta\delta + 32t_\perp\alpha\delta\xi)X_{N-1} - 8\xi\varepsilon D_N \\
&\quad + (16\delta^2 + 16\varepsilon^2 - 16\delta\xi)E_{N-1} + 8\delta\varepsilon D_{N-1} + (8U\delta\varepsilon - 16t_\perp\alpha\delta\varepsilon)Y_{N-1}, \\
D_{N+2} &= 2E_{N+1} - 4t_\perp\alpha Z_{N+1} - \beta D_{N+1} + 4t\xi Y_{N+1} - 2t_\perp\eta X_{N+1} + (-4t\varepsilon - 4t\delta)Y_N + 4t\alpha\delta X_N \\
&\quad + (16t\beta\delta + 8t\gamma\delta - 8U\xi\delta + 8t\eta\delta + 16t\beta\varepsilon)Z_{N-1} - 8\xi\delta E_{N-1} + 4\delta\varepsilon D_{N-1} + 4U\delta\varepsilon Y_{N-1}, \\
C_{N+2} &= 2\alpha E_{N+1} + (-4t_\perp + 2U\alpha)Z_{N+1} + 2t_\perp\beta Y_{N+1} + (-4t\xi + U\eta)X_{N+1} + \eta C_{N+1} \\
&\quad + 16t_\perp\xi\delta Z_{N-1} - 8t_\perp\delta\varepsilon Y_{N-1} + 4t\alpha\varepsilon Y_N. \tag{3}
\end{aligned}$$

APPENDIX II: THE DOPED LADDER

For the doped ladder (see Eq. 11), $|\phi_0\rangle_{N+2}$, $|\phi_1\rangle_{N+2}$, $|\phi_2\rangle_{N+1,N+2}$, $|\phi_3\rangle_{N+1,N+2}$, $|\phi_4\rangle_{N+1,N+2}$, $|\phi_5\rangle_{N+1,N+2}$, $|\phi_6\rangle_{N,N+1,N+2}$, and $|\phi_7\rangle_{N,N+1,N+2}$ are the same as the half-filled case, and

$$\begin{aligned}
|\phi_0^h\rangle_{N+2} &= |0\rangle_{N+2}, \\
|\phi_1\rangle_{N+1,N+2} &= \Delta_{(N+1,1),(N+2,2)}^\dagger |0\rangle_{N+1,N+2} + \Delta_{(N+2,1),(N+1,2)}^\dagger |0\rangle_{N+1,N+2}, \\
|\phi_2\rangle_{N+1,N+2} &= \Delta_{(N+1,1),(N+2,1)}^\dagger |0\rangle_{N+1,N+2} + \Delta_{(N+1,2),(N+2,2)}^\dagger |0\rangle_{N+1,N+2}, \\
|\phi_3\rangle_{N,N+1,N+2} &= \Delta_{(N,1),(N+2,1)}^\dagger \Delta_{(N+1,2),(N+2,2)}^\dagger |0\rangle_{N,N+1,N+2} + \Delta_{(N,2),(N+2,2)}^\dagger \Delta_{(N+1,1),(N+2,1)}^\dagger |0\rangle_{N,N+1,N+2}, \\
|\phi_4\rangle_{N,N+1,N+2} &= \Delta_{(N,1),(N+2,1)}^\dagger \Delta_{(N,2),(N+1,2)}^\dagger |0\rangle_{N,N+1,N+2} + \Delta_{(N,2),(N+2,2)}^\dagger \Delta_{(N,1),(N+1,1)}^\dagger |0\rangle_{N,N+1,N+2}. \tag{1}
\end{aligned}$$

To derive the recursion relations, we use the inner products from the half-filled case as well as the the following:

$$\begin{aligned}
&_{N+2}\langle\phi_0^h|\phi_0^h\rangle_{N+2}=1, \quad _{N+1,N+2}\langle\phi_1^h|\phi_1^h\rangle_{N+1,N+2}=4, \quad _{N+1,N+2}\langle\phi_2^h|\phi_2^h\rangle_{N+1,N+2}=4, \\
&_{N,N+1,N+2}\langle\phi_3^h|\phi_3^h\rangle_{N,N+1,N+2}=8, \quad _{N,N+1,N+2}\langle\phi_4^h|\phi_4^h\rangle_{N,N+1,N+2}=8, \\
&\langle N+1P+1|_{N+2}\langle\phi_0|\phi_3\rangle_{N,N+1,N+2}|N-1P\rangle=(-1)\langle N+1P+1|\phi_1\rangle_{N,N+1}|N-1P\rangle, \\
&\langle NP|_{N+1,N+2}\langle\phi_1^h|\phi_4^h\rangle_{N,N+1,N+2}|N-1P\rangle=(-2)\langle NP|\phi_0\rangle_N|N-1P\rangle. \tag{2}
\end{aligned}$$

Using these inner products, a straightforward calculation gives the following (coupled) recursion relations:

$$\begin{aligned}
Z_{N+2,P+1} &= (2+2\alpha^2)Z_{N+1,P+1} - 2\beta Y_{N+1,P+1} + 2\alpha\eta X_{N+1,P+1} + (4\beta^2 + 2\gamma^2 + 8\xi^2 + 2\eta^2)Z_{N,P+1} \\
&\quad + (16\delta^2 + 16\varepsilon^2 - 16\xi\delta)Z_{N-1,P+1} - 8\xi\varepsilon Y_{N,P+1} + 8\delta\varepsilon Y_{N-1,P+1} + \omega^2 Z_{N+1,P} + (4\lambda^2 + 4\zeta^2)Z_{N,P} \\
&\quad - 4\lambda\nu Y_{N,P} + (8\mu^2 + 8\nu^2 - 8\lambda\mu)Z_{N-1,P} + 4\mu\nu Y_{N-1,P}, \\
Y_{N+2,P+1} &= 2Z_{N+1,P+1} - \beta Y_{N+1,P+1} - 8\xi\delta Z_{N-1,P+1} + 4\delta\varepsilon Y_{N-1,P+1} - 4\mu\lambda Z_{N-1,P} + 2\mu\nu Y_{N-1,P},
\end{aligned}$$

$$\begin{aligned}
X_{N+2,P+1} &= 2\alpha Z_{N+1,P+1} + \eta X_{N+1,P+1}, \\
E_{N+2,P+1} &= (2 + 2\alpha^2)E_{N+1,P+1} + (-8t_\perp\alpha + 2U\alpha^2)Z_{N+1,P+1} - 2\beta D_{N+1,P+1} + 2\alpha\eta C_{N+1,P+1} \\
&\quad + (8t\xi + 4t_\perp\alpha\beta)Y_{N+1,P+1} + (-4t_\perp\eta - 8t\alpha\xi + 2U\alpha\eta)X_{N+1,P+1} \\
&\quad + (4\beta^2 + 2\gamma^2 + 8\xi^2 + 2\eta^2)E_{N,P+1} + (-32t\beta\xi + 4U\gamma^2 - 16t\gamma\xi + 8U\xi^2 - 16t\xi\eta + 4U\eta^2)Z_{N,P+1} \\
&\quad + (16t\beta\delta - 8t\varepsilon + 8t\alpha^2\varepsilon + 16t\beta\varepsilon + 8t\gamma\varepsilon - 8U\xi\varepsilon + 8t\eta\varepsilon - 8t\delta)Y_{N,P+1} + 8t\alpha\delta X_{N,P+1} \\
&\quad + (32t\beta\varepsilon + 16U\delta^2 + 16U\varepsilon^2 + 32t\beta\delta + 16t\gamma\delta - 16U\xi\delta + 16t\eta\delta + 32t_\perp\alpha\delta\xi)X_{N-1,P+1} - 8\xi\varepsilon D_{N,P+1} \\
&\quad + (16\delta^2 + 16\varepsilon^2 - 16\delta\xi)E_{N-1,P+1} + 8\delta\varepsilon D_{N-1,P+1} + (8U\delta\varepsilon - 16t_\perp\alpha\delta\varepsilon)Y_{N-1,P+1} \\
&\quad + E_{N+1,P} + (4\lambda^2 + 4\zeta^2)E_{N,P} + (8\mu^2 + 8\nu^2 - 8\lambda\mu)E_{N-1,P} - 4t\lambda Y_{N+1,P} - 4t\zeta X_{N+1,P} \\
&\quad + (-16t_\perp\lambda\zeta - 8t\lambda - 8t\alpha\zeta)Z_{N,P} + (4t\nu + 8t_\perp\zeta\nu + 4t\mu + 4t\nu)Y_{N,P} \\
&\quad + (-16t\beta\nu + 8t\mu + 16t_\perp\zeta\mu + 16t_\perp\alpha\lambda\mu - 16t\beta\mu)Z_{N-1,P} - 4\lambda\nu D_{N,P} + 4\mu\nu D_{N-1,P} \\
&\quad - 8t_\perp\alpha\mu\nu Y_{N-1,P}, \\
D_{N+2,P+1} &= 2E_{N+1,P+1} - 4t_\perp\alpha Z_{N+1,P+1} - \beta D_{N+1,P+1} + 4t\xi Y_{N+1,P+1} - 2t_\perp\eta X_{N+1,P+1} \\
&\quad + (-4t\varepsilon - 4t\delta)Y_{N,P+1} + 4t\alpha\delta X_{N,P+1} + (16t\beta\delta + 8t\gamma\delta - 8U\xi\delta + 8t\eta\delta + 16t\beta\varepsilon)Z_{N-1,P+1} \\
&\quad - 8\xi\delta E_{N-1,P+1} + 4\delta\varepsilon D_{N-1,P+1} + 4U\delta\varepsilon Y_{N-1,P+1} - 4t\lambda Z_{N,P} + (2t\nu + 2t\mu)Y_{N,P} \\
&\quad - 4\lambda\mu E_{N-1,P} + 2\mu\nu D_{N-1,P} + (4t\mu + 8t_\perp\zeta\mu)Z_{N-1,P}, \\
C_{N+2,P+1} &= 2\alpha E_{N+1,P+1} + (-4t_\perp + 2U\alpha)Z_{N+1,P+1} + 2t_\perp\beta Y_{N+1,P+1} + (-4t\xi + U\eta)X_{N+1,P+1} \\
&\quad + \eta C_{N+1,P+1} + 16t_\perp\zeta\delta Z_{N-1,P+1} - 8t_\perp\delta\varepsilon Y_{N-1,P+1} + 4t\alpha\varepsilon Y_{N,P+1} - 4t\zeta Z_{N,P} \\
&\quad + 8t_\perp\lambda\mu Z_{N-1,P} - 4t_\perp\mu\nu Y_{N-1,P}.
\end{aligned} \tag{3}$$

¹ For a review see E. Dagotto and T. M. Rice, *Science* **271**, 618 (1996).

² For example see C. Varma and A. Zawadowski, *Phys. Rev. B* **32**, 7399 (1985), D. G. Shelton, A. A. Nersesyan, and A. M. Tsvelik, *Phys. Rev. B* **53**, 8521 (1996), H. H. Lin, L. Balents, and M. P. A. Fisher, *Phys. Rev. B* **58**, 1794 (1998), and references therein.

³ For example see T. M. Rice, S. Haas, M. Sigrist, and F. C. Zhang, *Phys. Rev. B* **56**, 14655 (1997), R. M. Noak, S. R. White, and D. J. Scalapino, *Physica C* **270**, 281 (1996), and references therein.

⁴ Z. Hiroi, M. Azuma, M. Takano, and Y. Bando, *J. Solid State Chem.* **95**, 230 (1991), M. Uehara, *et. al.*, *J. Phys. Soc. Jpn.* **65**, 2764 (1996) and references therein.

⁵ D. C. Johnston, *et. al.*, *Phys. Rev. B* **35**, 219 (1987); R. S. Eccleston, *et. al.*, *Phys. Rev. Lett.* **73**, 2626 (1994).

⁶ M. Takano, *et. al.*, *J. Solid State Chem.* **95**, 230 (1991); M. Azuma, *et. al.*, *Phys. Rev. Lett.* **73**, 3463 (1994).

⁷ M. Azuma, *et. al.*, *Phys. Rev. Lett.* **73**, 3463 (1994).

⁸ G. Sierra and M. A. Martin-Delgado, *Phys. Rev. B* **56**, 8774 (1997).

⁹ G. Sierra, M. A. Martin-Delgado, J. Dukelsky, S. R. White,

and D. J. Scalapino, *Phys. Rev. B* **57**, 11666 (1998).

¹⁰ K. G. Wilson, *Rev. Mod. Phys.* **47**, 773 (1975).

¹¹ S. R. White, *Phys. Rev. Lett.* **69**, 2863 (1992); S. R. White, *Phys. Rev. B* **48**, 10345 (1993).

¹² S. R. White, R. M. Noack, and D. J. Scalapino, *Phys. Rev. Lett.* **73**, 886 (1994).

¹³ Note that $|\phi_i\rangle_{N+2,N+1} |N\rangle$ should (more precisely) be written $|\phi_i\rangle_{N+2,N+1} \otimes |N\rangle$. However, throughout the paper, to make things less notationally cumbersome, we have omitted the tensor product symbol.

¹⁴ D. J. Scalapino and S. A. Trugman, *Phil. Mag. B* **74**, 607 (1996).

¹⁵ S. R. White and D. J. Scalapino, *Phys. Rev. B* **55**, 6504 (1997).

¹⁶ S. Daul and R. M. Noack, private communication. The accuracy for the DMRG groundstate energy is 10^{-5} .

¹⁷ E. Jeckelmann, D. J. Scalapino, and S. R. White, *Phys. Rev. B* **58**, 9492 (1998).

¹⁸ G. Fano, F. Ortolani, and L. Ziosi, *Phys. Rev. B* **54**, 17557 (1996); A. Messager and J. L. Richard, *Phys. Lett. A* **143**, 345 (1990); G. M. Cicuta and S. Stramaglia, *Phys. Lett. A* **165**, 456 (1992).

¹⁹ S. Östlund and S. Rommer, *Phys. Rev. Lett.* **75**, 3537 (1995); S. Östlund and S. Rommer, *Phys. Rev. B* **55**, 2164 (1997).

²⁰ J. M. Roman, G. Sierra, J. Dukelsky, and M. A. Martin-Delgado, *J. Phys. A: Math. Gen.* **31**, 9729 (1998).